THE JOURNAL OF PHYSICAL CHEMISTRY C

Article

pubs.acs.org/JPCC

Lattice-Directed Construction of Metal–Organic Molecular Wires of Pentacene on the Au(110) Surface

Junhai Ren,[†,§] De-Liang Bao,[†,§] Li Dong,[†] Lei Gao,[†] Rongting Wu,[†] Linghao Yan,[†] Aiwei Wang,[†] Jiahao Yan,[†] Yeliang Wang,[†,‡] Qing Huan,[*,†,‡] Jia-Tao Sun,[†] Shixuan Du,[*,†,‡] and Hong-Jun Gao[†,‡]

[†]Institute of Physics, Chinese Academy of Sciences, and University of Chinese Academy of Sciences, Beijing 100190, P. R. China

[‡]Beijing Key Laboratory for Nanomaterials and Nanodevices, Beijing 100190, P. R. China

S *Supporting Information*

ABSTRACT: The construction of metal–organic molecular wires is important for the design of specific functional devices but has been a great challenge for experimental technology. Here we report the formation of one-dimensional metal–organic structures by direct deposition of pentacene molecules on the Au(110) surface with subsequent thermal annealing. These metal–organic molecular wires were systematically explored by scanning tunneling microscopy (STM) and density functional theory calculations. At submonolayer coverage, during annealing at ∼470 K, the adsorbed molecules induce both Au(110)-(1 × 3) surface reconstruction, where two atomic rows are missing every three rows on the Au(110) surface, with the end-to-end pentacene configuration and Au(110)-(1 × 6) surface reconstruction, where five rows are missing every six rows on the surface, with the side-by-side configuration. Further annealing at ∼520 K results in Au-adatom-coordinated metal–organic molecular wires with a new side-by-side configuration of pentacene molecules on the Au(110)-(1 × 6) surface. The Au adatoms linking neighboring pentacene molecules, indicated by bright features in the STM image, were strongly evidenced by the STM simulations. Therefore, metal–organic molecular wires of pentacene on Au(110) were achieved through coordination bonds between native Au atoms and the −CH− groups of pentacene molecules.

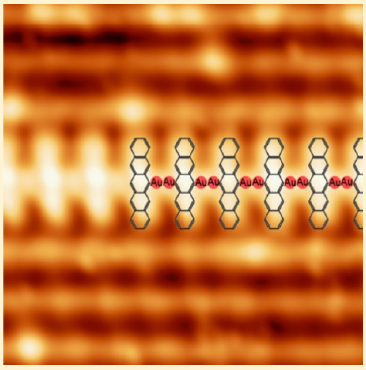

INTRODUCTION

The construction of diverse metal–organic frameworks (MOFs) has aroused much interest in the past two decades because of their extraordinary properties such as ultrahigh porosity,[1−5] enormous internal surface area,[4,5] ease of use in clean energy,[1,3,5] controllable performance in nanodevices,[4,6] etc. Accordingly, on-surface reaction in an ultrahigh vacuum (UHV) environment has been utilized to construct low-dimensional metal–organic compounds, for example, one-dimensional (1D) molecular wires or two-dimensional (2D) networks, by hierarchical molecular assembly linked with metal atoms.[7−15] Importantly, because 1D metal–organic molecular wires can confine the carriers moving along the wire, they have potential applications in anisotropic-transport-based devices.[16−18] Compared with pure metal wires, metal–organic molecular wires have weaker coupling with the substrate, better mechanical stability, and better compatibility with the traditional metal electrodes.

In previous work, almost all 1D organometallic structures were constructed by precursors with functional groups such as halogen,[19] carboxyl,[2,20,21] pyridyl,[10,22] carbonitrile,[7,23] alkynyl, etc.[24−26] Although these functional groups are beneficial for physical or chemical bonding between molecules and metal atoms, the additional groups can bring complexity and uncertainty to the electronic properties of the molecular skeletons. For example, because of fascinating properties arising from their suitable HOMO–LUMO gap and delocalized π-electronic structures, pentacene molecules have been widely utilized to construct nanodevices,[27] organic field-effect transistors (OFETs),[28,29] organic photovoltaic cells (OPVs),[30] etc. However, in these devices, functional ligand groups usually influence the electronic properties of the pentacene molecules significantly.[31−34] Construction of metal–organic molecular wires without changing the intrinsic electronic properties of the organic molecule is still challenging. Repp et al. reported that coordination bonds can be formed between Au atoms and −CH− groups in pentacene.[35] However, the construction of 1D molecular wires that consists of aromatic hydrocarbons and metal atoms without dehydrogenation has rarely been reported.

Furthermore, a well-defined template to construct 1D molecular wires is also important. It is interesting to note that the Au(110) surface has missing-row reconstruction, which can be used as a template to construct one-dimensional structures. Remarkably, the Au(110)-(1 × 2) surface reconstruction is strongly influenced by doping or adsorbates. The width of the missing-row reconstruction can be self-adapted to the size of the adsorbates. Meanwhile, understanding the interaction mechanism between Au(110) and the adsorbates will be helpful for constructing 1D molecular wires.

Received: April 27, 2017
Revised: September 12, 2017
Published: September 12, 2017

DOI: 10.1021/acs.jpcc.7b03957
J. Phys. Chem. C 2017, 121, 21650−21657

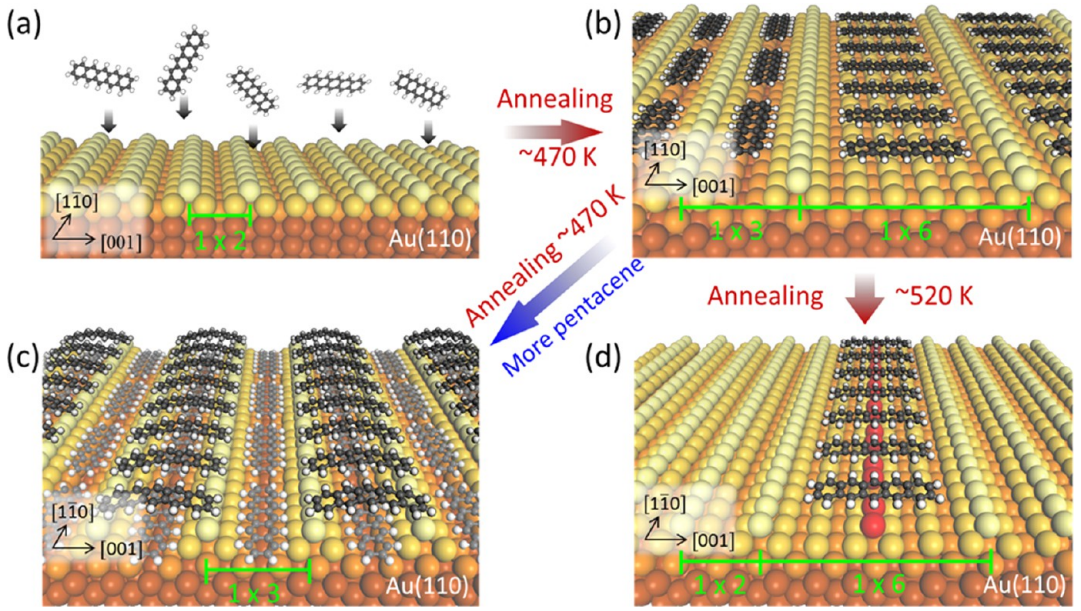

Figure 1. Schematic illustrations of the self-assembly behaviors of pentacene molecules deposited on the Au(110) surface (a) with the intrinsic (1 × 2) surface reconstruction, (b, d) after annealing of the sample to (b) about 470 K and (d) about 520 K, and (c) with more than 1 ML of pentacene molecules deposited onto the Au(110) surface after annealing at 470 K.

In this paper, combining scanning tunneling microscopy (STM) measurements and density functional theory (DFT) calculations, we report the formation of one-dimensional Au−pentacene molecular wires on the reconstructed Au(110) missing-row surface by control of the pentacene coverage and annealing temperature. At low coverage and an annealing temperature of about 470 K, pentacene molecules adopt two configurations with their long molecular axes parallel or normal to the [1$\bar{1}$0] direction of the underlying Au(110) substrate, corresponding to the Au(110)-(1 × 3) and Au(110)-(1 × 6) surface reconstructions, respectively. The Au(110)-(1 × n) is defined as the new period of the Au(110) surface induced by missing-row reconstruction, where n is the multiple of the reconstructed period relative to the original Au(110)-(1 × 1) surface. Notably, after the sample is annealed to about 520 K, pentacene molecules can form one-dimensional Au−pentacene organometallic molecular wires along the [1$\bar{1}$0] direction of the Au(110) substrate. The STM simulations show good agreement with the experimental images. Further calculations prove that a strong chemical interaction can occur between pentacene molecules and coordinated Au atoms. Moreover, at high coverage the pentacene molecules form an arched bilayer structure by vertical stacking.

METHODS

Experimental Section. Our experiments were carried out in a homemade UHV variable-temperature (VT) STM system with a base pressure better than 2.0 × 10^{-10} Torr, as described elsewhere.[36] Single-crystal Au(110) (purchased from MaTeck Company) was treated in the UHV chamber by repeated cycles of Ne^+ sputtering and subsequent annealing at about 850 K until the well-known (1 × 2) reconstruction of the Au(110) surface was observed by STM imaging. A refinement and degassing process for pentacene molecules was necessary before they could be deposited on the Au(110) surface. Commercial pentacene samples were first purified by sublimation in a homemade Knudsen cell evaporator in high vacuum for several days and then further refined by degassing at about 390 K for several hours under UHV conditions. At last, molecules at about 370 K were deposited on the clean Au(110) surface while the substrate was kept at 100 K. The deposition rate was about 0.1 ML/min. Herein, one monolayer (ML) refers to the amount of deposited pentacene molecules that completely covers the substrate surface. All of the STM images were obtained in constant-current mode. All voltages given refer to the sample. The sample and tip were kept at 100 K.

Calculation Details. To deepen our understanding, we turned to DFT calculations performed with the Vienna Ab Initio Simulation Package (VASP)[37] using the projector augmented wave (PAW) method[38] to describe the interaction between the ions and electrons and the Perdew−Burke−Ernzerhof (PBE)[39] generalized gradient approximation (GGA)[40] for the exchange−correlation function. The unit cells for calculation models were built with (3 × 6) and (6 × 3) supercells of Au(110) for horizontal and vertical configurations, respectively. The substrate was modeled with a slab of five atomic layers, isolated in the z direction by more than 15 Å of vacuum. The two bottom layers of Au atoms were fixed, while the other Au atoms and the on-top molecules were fully relaxed until the force for the nonfixed atoms was less than 0.02 eV/Å. The energy cutoff of the plane-wave basis sets was 400 eV, and k-point sampling was done only at the Γ point. Van der Waals (vdW) interactions were included by using the dispersion-corrected DFT-D2 method of Grimme.[41] The STM simulations were based on the Tersoff−Hamann approximation. Within this approximation, the STM image is a contour of the local density of states (LDOS) of the system. The charge density differences were calculated as $\Delta\rho = \rho_{tot} - \rho_{sub} - \rho_{mol}$, where ρ_{tot} is the charge density of the total system, ρ_{sub} is the electron density of the Au(110) substrate, and ρ_{mol} is the electron density of the pentacene molecule. The charge density differences $\Delta\rho$ show the charge redistribution induced by the interaction between the molecule and the substrate.

DOI: 10.1021/acs.jpcc.7b03957
J. Phys. Chem. C 2017, 121, 21650−21657

RESULTS AND DISCUSSION

Figure 1 illustrates the basic procedure for the assembly of pentacene molecules on the Au(110) missing-row surface reconstruction. First, pentacene molecules are deposited onto the Au(110) surface at lower coverage (see Figure 1a). While the sample is annealed at about 470 K, two different self-assembly behaviors occur, inducing (1 × 3) and (1 × 6) surface reconstructions, as shown in Figure 1b. The subsequent annealing procedure gives rise to Au-adatom-coordinated metal−organic molecular wires (see Figure 1d). In addition, depositing more pentacene molecules allows self-regulated growth and ripening of bilayer structures (see Figure 1c).

Figure 2a shows an STM image after deposition of less than one monolayer (ML) of pentacene molecules onto the Au(110) surface and subsequent annealing of the sample to about 470 K for 1 h. The black rows in Figure 2a represent the intrinsic Au(110)-(1 × 2) surface reconstruction,[42] as can be ascertained by the distance of 0.82 nm between two neighboring rows, which is about $2\sqrt{2}$ times the Au−Au bond length (0.29 nm). There is a wider channel with a width of 1.21 nm (green marks in Figure 2a), which is $3\sqrt{2}$ times the Au−Au bond length, indicating the formation of the induced Au(110)-(1 × 3) surface reconstruction. A pentacene molecule has a short strip shape covered by a molecular skeleton. Pentacene molecules are assembled end-to-end in the (1 × 3) surface channels with each molecule's long axis along the [1$\bar{1}$0] direction of the substrate. In addition, in the right portion of Figure 2a, the channel with a width of 2.39 nm (yellow marks in Figure 2a) represents the induced Au(110)-(1 × 6) surface reconstruction, wherein pentacene molecules are assembled side-by-side with their long axes along the [001] direction of the substrate. These two growth modes are consistent with the previous indirect evidence coming from X-ray photoemission spectroscopy (XPS) and low-energy electron diffraction (LEED) measurements. The high-resolution STM images of self-assembly structures of pentacene molecules on Au(110) surface at monolayer coverage shown in Figure 2 provide the direct observations.[43−49] By conducting statistical analysis in several different areas on the sample, we found the percentage of the Au(110)-(1 × 3) surface reconstruction to be about 80%, as shown in Figure S1.

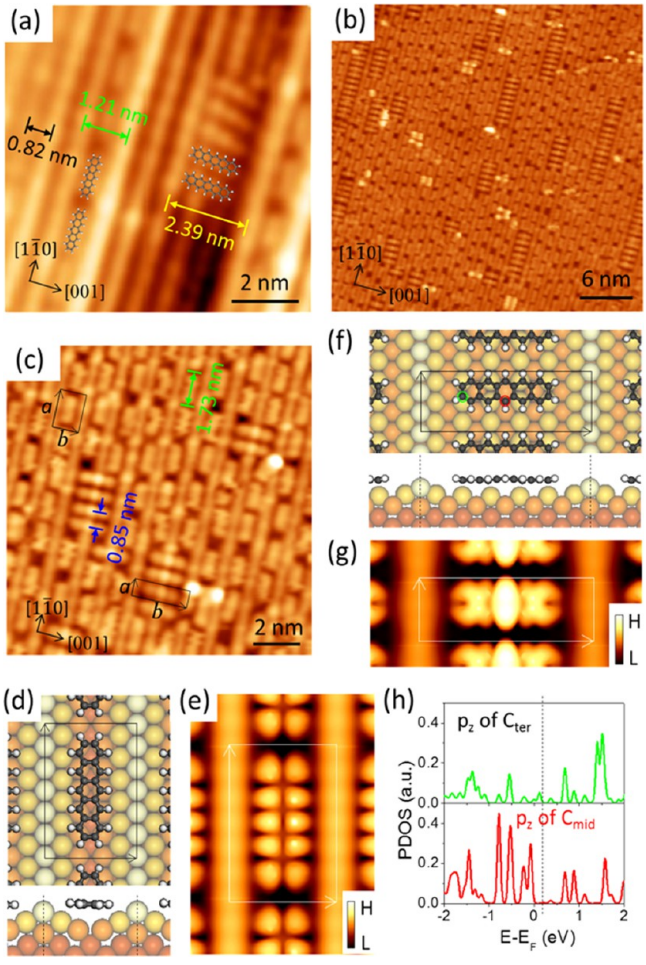

Figure 2. Analysis of two distinct topographies for pentacene molecules on the Au(110) surface. (a) STM image after pentacene deposition on Au(110) at low coverage. (b) STM image of the pentacene monolayer film. (c) Zoomed-in STM image of the two different topographies for pentacene molecules. (d, e) Structural model and simulated STM image of pentacene molecules in the (1 × 3) reconstructed channel. (f, g) Structural model and simulated STM image of pentacene molecules in the (1 × 6) reconstructed channel. (h) Projected DOS of the p_z orbital of a middle C atom and the p_z orbital of a terminal C atom of a pentacene molecule. The scanning parameters were −0.6 V, 0.1 nA in (a), −0.5 V, 0.1 nA in (b), and −0.53 V, 0.1 nA in (c).

After deposition of more pentacene molecules onto the Au(110) surface to 1 ML and annealing of the sample to about 470 K, ordered self-assembly of monolayer pentacene molecules occurs, as shown in Figure 2b. The pentacene molecules exhibit an ordered distribution on the substrate with end-to-end and side-by-side configurations on the Au(110)-(1 × 3) and Au(110)-(1 × 6) surface reconstructions, respectively, while the intrinsic (1 × 2) surface reconstruction has completely disappeared. The magnified STM image of monolayer pentacene molecules in Figure 2c shows that the pentacene molecules have two growth modes, both following the Au atomic rows. The distance between two adjacent end-to-end molecules is 1.73 nm (green marks in Figure 2c), about 6 times as long as the Au−Au bond length, indicating a (6 × 3) superlattice commensurate with the Au(110) substrate. For side-by-side molecules, the distance is 0.85 nm (blue marks in Figure 2c), about 3 times the Au−Au bond length, indicating a (3 × 6) self-assembled superlattice with respect to the Au(110) substrate.

In order to better understand the adsorption configuration of the molecules on the surface, DFT calculations were carried out, and the results are illustrated in Figure 2d−h. Our calculations indicate that the (1 × 3) and (1 × 6) surface reconstruction channels are compatible with the short and long axes of the pentacene molecules, which reorganize into these reconstructed channels. Simulated STM images of the two configurations (Figure 2e,g) agree with the experimental images very well. It is worthy of mention that the little bright feature in the middle of the side-by-side configuration in Figure 2c is due to the localized electron states of the C atom in the middle of the pentacene molecule. The projected densities of states (PDOS) of the p_z orbital of the middle C atom (C_{mid}) and the p_z orbital of a terminal C atom (C_{ter}) of a pentacene molecule are shown in Figure 2h. Obviously, in the energy range from −1 eV to the Fermi level, more electrons in p_z orbitals are distributed on C_{mid} than on C_{ter}, indicating a distinct interaction at the −CH−/substrate interface. This is also reflected in the

DOI: 10.1021/acs.jpcc.7b03957
J. Phys. Chem. C 2017, 121, 21650−21657

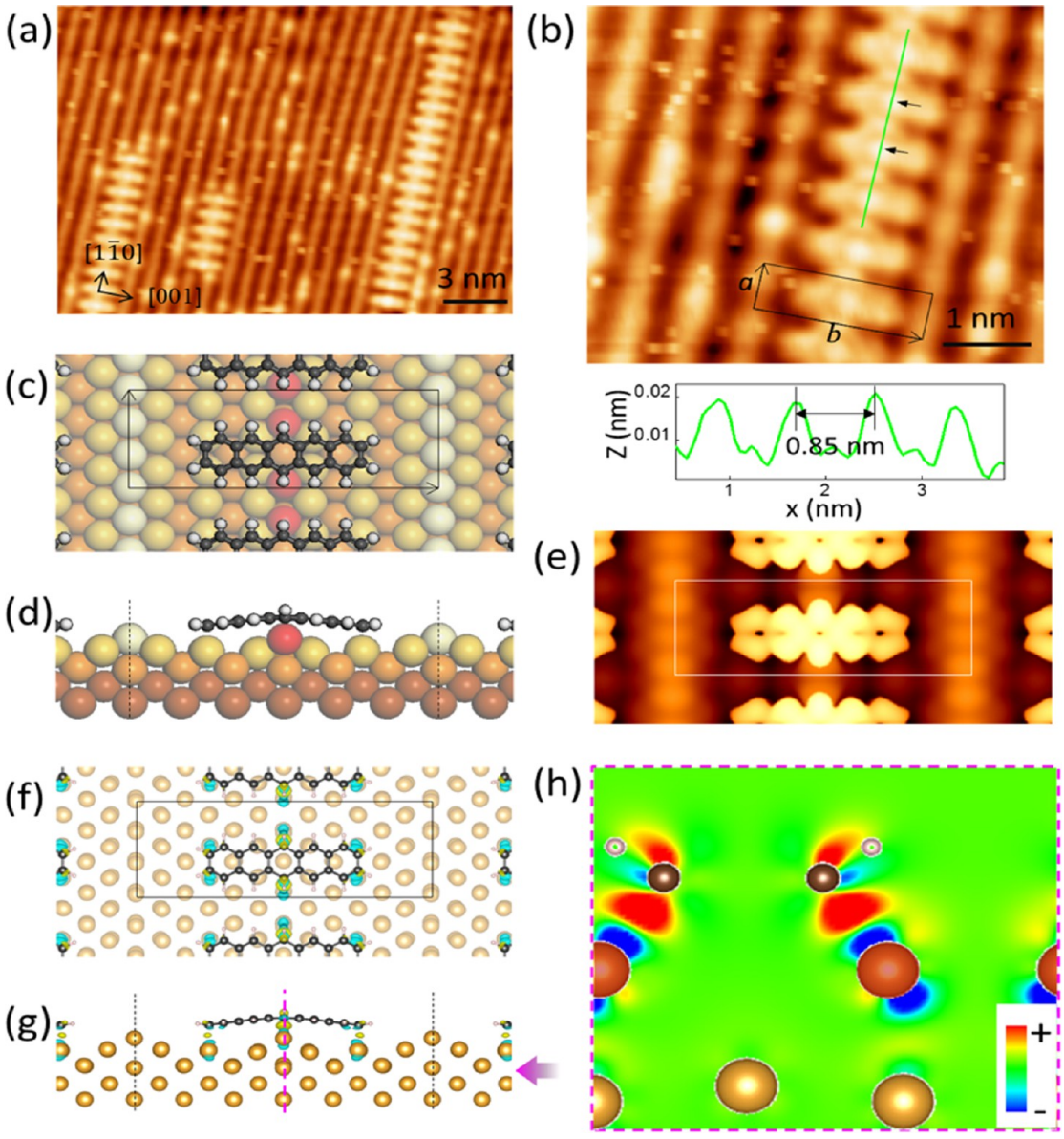

Figure 3. Structure of 1D pentacene−gold structures achieved through annealing of the monolayer thin film at about 520 K. (a) Large-scale STM image of the pentacene−gold molecular wires on Au(110). (b) Zoomed-in STM image of the structure. The lower panel shows a line profile along the [1$\bar{1}$0] direction. (c, d) Top and side views of the structural model of the pentacene−gold molecular wires on Au(110). (e) Theoretical simulated STM image based on the model in (c, d). (f, g) Top and side views of the charge density difference of the pentacene−gold metal−organic molecular wires. Yellow represents gain of electrons, and blue represents loss of electrons. The value of the isosurface is 0.036 e/Å^3. (h) Cross-sectional view of the charge density difference in (f, g) along the violet dashed line in (g). The scanning parameters were −0.46 V, 0.1 nA in (a) and −0.67 V, 0.1 nA in (b).

simulated STM image shown in Figure 2g, which matches the STM image quite well.

When the sample was annealed at about 520 K for 1 h, the surface structures changed a lot, as shown in Figure 3a. Because of the thermal motion, most of the pentacene molecules are desorbed from the substrate. The exposed parts of the Au(110) surface revert to the (1 × 2) surface reconstruction. Notably, the remaining pentacene molecules arrange themselves in side-by-side mode parallel to the [1$\bar{1}$0] direction of the substrate, located in the (1 × 6) surface reconstruction, with a string of bright dots lined up through the middle of them. The high-resolution STM image is shown in Figure 3b. The bright feature between two adjacent pentacene molecules is very distinct from the dark feature observed in the monolayer sample, as shown in Figure 2c. A Au−pentacene molecular wire, in which several Au adatoms are stuck between two pentacene molecules, is formed. The (1 × 3) phases transformed to (1 × 6) phases, which is required prior to the formation of the 1D molecular wire.

The atomic configuration of the 1D molecular wire is shown in Figure 3c,d. As shown by the line profile in Figure 3b, the distance between two neighboring pentacene molecules is 0.85 nm, the same as in Figure 2c, indicating a (3 × 6) superlattice with respect to the Au(110) substrate. Because of the distinct interface interaction between the −CH− groups and the substrate, as discussed above, thermally diffusing Au atoms on the surface are captured here, interacting strongly with the middle −CH− parts of pentacene molecules. That is why these

DOI: 10.1021/acs.jpcc.7b03957
J. Phys. Chem. C 2017, 121, 21650−21657

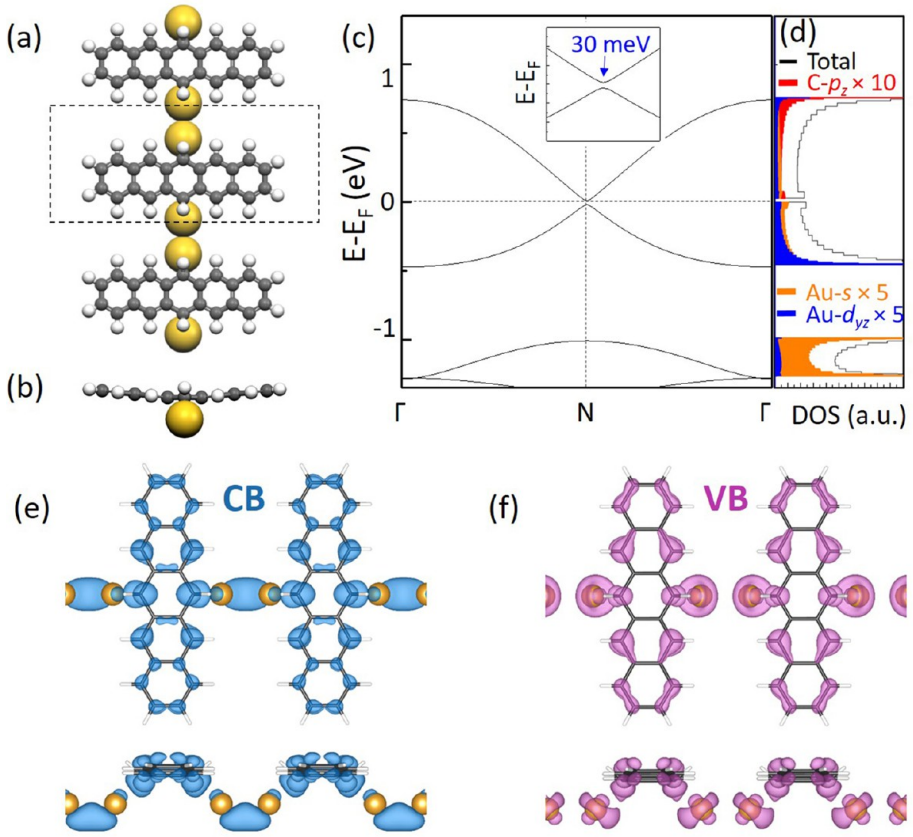

Figure 4. Configuration and electronic structure of a freestanding metal−organic molecular wire. (a) Top view and (b) side view of a freestanding Au−pentacene molecular wire. (c) Band structure and (d) density of states (DOS) of the Au−pentacene molecular wire. In (d), the black curve is the total DOS, the orange and blue shadows are the DOS projected on the s and d_{yz} orbitals of Au atom, respectively, and the red shadow is the DOS projected on the p_z orbital of the C atom bonding to the Au atom. In (c), a small band gap near the Fermi level is shown in the zoomed-in figure. (e, f) Electron distributions of (e) the conduction band (CB) and (f) the valence band (VB). The isosurface is 0.003 e/bohr^3.

molecules in side-by-side configurations did not desorb at high temperature as others did. In Figure 3c,d, two Au adatoms can be seen located at the hollow sites in the −CH−/substrate interface, between any two pentacene molecules, bonded to the C_{mid} atoms with a bond length of 2.25 Å. The middle of the molecule humps up, both ends of the molecules are bent toward the substrate, and the middle two H atoms are upturned a little. This bonding configuration is determined by the simulated STM image (Figure 3e), which matches the experimental image in Figure 3b quite well. The simulated STM images of other possible configurations do not agree with the experimental images so well, as shown in Figure S2.

To investigate the interaction between pentacene molecules and coordinated Au adatoms, we calculated the charge density difference between the molecule and the substrate; the top view is shown in Figure 3f, and the side view is shown in Figure 3g. Figure 3h is a cross-sectional view of the charge density difference through the two middle C atoms and two Au adatoms, along the violet dashed line in Figure 3g. This indicates the significant charge rearrangement between the Au adatoms and the middle C atoms. According to previous reports,[35,50] a covalent bond between a single Au atom and a pentacene molecule can be formed. Therefore, in our case, as a result of the template effect of the Au(110) surface, a perfectly straight, defect-free 1D metal−organic molecular wire forms through coordination between native Au adatoms and the middle −CH− groups of pentacene molecules. Moreover, from the simulated STM image one can see that the conjugated molecular orbital has not changed much. As a result of the delicate molecule−substrate interplay, one can grow a large variety of analogous 1D polymers using an anisotropic metal surface as both the substrate and template, which is of great significance for the surface engineering of novel devices.

The atomic configuration and electronic structure of a freestanding metal−organic molecular wire are shown in Figure 4. The band structure shows that the freestanding metal−organic molecular wire is a semiconductor with a small band gap of 30 meV at the Fermi level (Figure 4c). The conduction band (CB) and valence band (VB) are mainly contributed from the hybridization of the s and d_{yz} orbitals of Au and the p_z orbital of the C atom bonded to the Au atom. The electron distributions of the CB and VB (Figure 4e,f, respectively) reveal that the electrons and holes are delocalized, indicating good electron and hole conductivity. The dispersion near the CB minimum (CBM) and VB maximum (VBM) is strong, indicating high carrier mobility. Moreover, the molecular wire we obtained has a narrow width (~1 nm), which means that the scattering of the current carriers is weak. Therefore, long-distance transport can be achieved and protected inside the molecular wire.

When we deposit more pentacene molecules onto the self-assembled monolayer shown in Figure 2b,c and then anneal the sample at low temperature (about 470 K), we find that the newly deposited molecules assemble upon the first layer, all in the side-by-side mode, as shown in Figure 5a,b. The bottom-layer molecules are still located in both the (1 × 3) and (1 × 6)

DOI: 10.1021/acs.jpcc.7b03957
J. Phys. Chem. C 2017, 121, 21650−21657

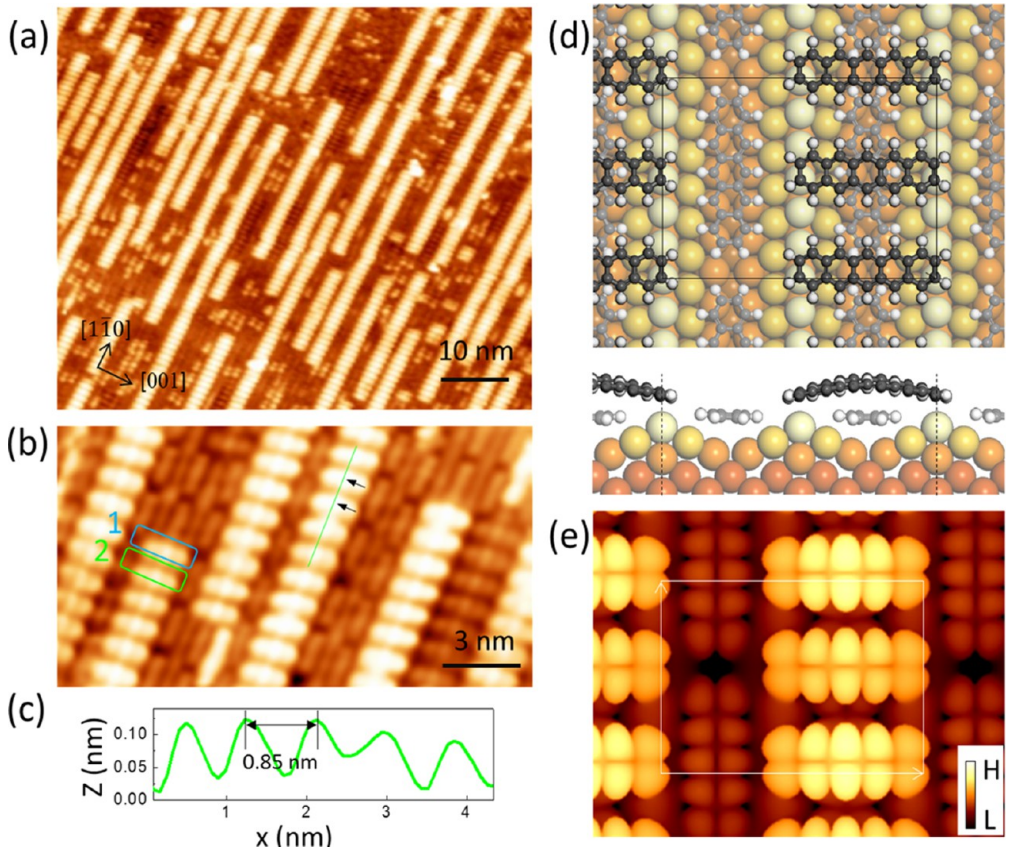

Figure 5. Structure of pentacene molecules on the Au(110) surface at bilayer coverage. (a) Large-scale STM image of this bilayer structure. (b) Zoomed-in STM image of the bilayer structure. (c) Profile along the [1$\bar{1}$0] direction in (b). (d, e) Structural model and simulated STM image of the pentacene bilayer structure on Au(110). The scanning parameters in both (a) and (b) were −0.53 V, 0.1 nA.

surface-reconstructed channels, whereas the second-layer molecules are preferentially situated on top of the (1 × 3) channels. The distance between neighboring molecules in the line profile shown in Figure 5c is still 0.85 nm, a suitable van der Waals interaction distance for pentacene molecules. The second layer of pentacene molecules is stable below 470 K and desorbs at higher temperature. DFT calculations were carried out, and the results are shown in Figure 5d,e. The molecules in the second layer do not adsorb flat on the monolayer thin film but are configured in a low arch, and the simulated STM image (Figure 5e) matches the experimental images quite well.

CONCLUSION

At about 470 K, pentacene molecules can induce both Au(110)-(1 × 3) surface reconstruction with the end-to-end molecular configuration and Au(110)-(1 × 6) surface reconstruction with the side-by-side configuration with coverage ranging from submonolayer to monolayer. Importantly, we used the special lattice feature of the anisotropic Au(110) substrate to successfully construct one-dimensional metal−organic molecular wires consisting of pentacene molecules with Au adatoms at about 520 K. These metal−organic molecular wires are not only straight and free of defects but also retain the conjugation property of pentacene molecules. In a second layer, pentacene molecules adopt only the side-by-side configuration on top of pentacene molecules in the (1 × 3) surface reconstruction at about 470 K, which reveals detailed interface information about the initial growth of the pentacene crystal system on metals.

ASSOCIATED CONTENT

Supporting Information

The Supporting Information is available free of charge on the ACS Publications website at DOI: 10.1021/acs.jpcc.7b03957.

STM images and structures considered for Au(110)-(1 × 6) reconstruction (PDF)

AUTHOR INFORMATION

Corresponding Authors

*E-mail: sxdu@iphy.ac.cn.

*E-mail: huanq@iphy.ac.cn.

ORCID

Junhai Ren: 0000-0002-5948-1967

Shixuan Du: 0000-0001-9323-1307

Author Contributions

§J.R. and D.-L.B. contributed equally to this work.

Notes

The authors declare no competing financial interest.

ACKNOWLEDGMENTS

We thank Werner A. Hofer, Sokrates T. Pantelides, and Min Ouyang for constructive suggestions. We acknowledge financial support from the National Key Research & Development Projects of China (2016YFA0202300), the National Basic Research Program of China (2013CBA01600), the National Natural Science Foundation of China (61390501, 61471337, 61622116, and 51325204), the National Key Scientific Instrument and Equipment Development Project of China

DOI: 10.1021/acs.jpcc.7b03957
J. Phys. Chem. C 2017, 121, 21650−21657

(2013YQ1203451), the CAS Hundred Talents Program, the Transregional Collaborative Research Center TRR 61 (21661132006), and the National Supercomputing Center in Tianjin. A portion of the research was performed at the CAS Key Laboratory of Vacuum Physics.

REFERENCES

(1) Mueller, U.; Schubert, M.; Teich, F.; Puetter, H.; Schierle-Arndt, K.; Pastre, J. Metal-Organic Frameworks - Prospective Industrial Applications. *J. Mater. Chem.* **2006**, *16*, 626−636.

(2) Stepanow, S.; Lin, N.; Barth, J. V.; Kern, K. Surface-Template Assembly of Two-Dimensional Metal-Organic Coordination Networks. *J. Phys. Chem. B* **2006**, *110*, 23472−23477.

(3) O'Keeffe, M.; Yaghi, O. M. Deconstructing the Crystal Structures of Metal-Organic Frameworks and Related Materials into Their Underlying Nets. *Chem. Rev.* **2012**, *112*, 675−702.

(4) Furukawa, H.; Cordova, K. E.; O'Keeffe, M.; Yaghi, O. M. The Chemistry and Applications of Metal-Organic Frameworks. *Science* **2013**, *341*, 1230444.

(5) Eddaoudi, M.; Kim, J.; Rosi, N.; Vodak, D.; Wachter, J.; O'Keeffe, M.; Yaghi, O. M. Systematic Design of Pore Size and Functionality in Isoreticular MOFs and Their Application in Methane Storage. *Science* **2002**, *295*, 469−472.

(6) Talin, A. A.; Centrone, A.; Ford, A. C.; Foster, M. E.; Stavila, V.; Haney, P.; Kinney, R. A.; Szalai, V.; El Gabaly, F.; Yoon, H. P.; et al. Tunable Electrical Conductivity in Metal-Organic Framework Thin-Film Devices. *Science* **2014**, *343*, 66−69.

(7) Tait, S. L.; Langner, A.; Lin, N.; Chandrasekar, R.; Fuhr, O.; Ruben, M.; Kern, K. Assembling Isostructural Metal-Organic Coordination Architectures on Cu(100), Ag(100) and Ag(111) Substrates. *ChemPhysChem* **2008**, *9*, 2495−2499.

(8) Shi, Z. L.; Lin, N. Porphyrin-Based Two-Dimensional Coordination Kagome Lattice Self-Assembled on a Au(111) Surface. *J. Am. Chem. Soc.* **2009**, *131*, 5376−5377.

(9) Shi, Z. L.; Lin, N. Structural and Chemical Control in Assembly of Multicomponent Metal-Organic Coordination Networks on a Surface. *J. Am. Chem. Soc.* **2010**, *132*, 10756−10761.

(10) Li, Y.; Xiao, J.; Shubina, T. E.; Chen, M.; Shi, Z.; Schmid, M.; Steinruck, H. P.; Gottfried, J. M.; Lin, N. Coordination and Metalation Bifunctionality of Cu with 5,10,15,20-Tetra(4-pyridyl)porphyrin: Toward a Mixed-Valence Two-Dimensional Coordination Network. *J. Am. Chem. Soc.* **2012**, *134*, 6401−6408.

(11) Xie, Y.-c.; Rokni Fard, M.; Kaya, D.; Bao, D.; Palmer, R. E.; Du, S.; Guo, Q. Site-Specific Assembly of Fullerene Nanorings Guided by Two-Dimensional Gold Clusters. *J. Phys. Chem. C* **2016**, *120*, 10975−10981.

(12) Langner, A.; Tait, S. L.; Lin, N.; Rajadurai, C.; Ruben, M.; Kern, K. Self-Recognition and Self-Selection in Multicomponent Supramolecular Coordination Networks on Surfaces. *Proc. Natl. Acad. Sci. U. S. A.* **2007**, *104*, 17927−17930.

(13) Langner, A.; Tait, S. L.; Lin, N.; Chandrasekar, R.; Ruben, M.; Kern, K. Ordering and Stabilization of Metal-Organic Coordination Chains by Hierarchical Assembly through Hydrogen Bonding at a Surface. *Angew. Chem., Int. Ed.* **2008**, *47*, 8835−8838.

(14) Langner, A.; Tait, S. L.; Lin, N.; Chandrasekar, R.; Ruben, M.; Kern, K. Two- to One-Dimensional Transition of Self-Assembled Coordination Networks at Surfaces by Organic Ligand Addition. *Chem. Commun.* **2009**, 2502−2504.

(15) Tseng, T. C.; Lin, C. S.; Shi, X. Q.; Tait, S. L.; Liu, X.; Starke, U.; Lin, N.; Zhang, R. Q.; Minot, C.; Van Hove, M. A.; Cerda, J. I.; Kern, K. Two-Dimensional Metal-Organic Coordination Networks of Mn-7,7,8,8-Tetracyanoquinodimethane Assembled on Cu(100): Structural, Electronic, and Magnetic Properties. *Phys. Rev. B: Condens. Matter Mater. Phys.* **2009**, *80*, 155458.

(16) Choi, S. H.; Kim, B.; Frisbie, C. D. Electrical Resistance of Long Conjugated Molecular Wires. *Science* **2008**, *320*, 1482−1486.

(17) Wan, W. M. V.; Greenham, N. C.; Friend, R. H. Interference Effects in Anisotropic Optoelectronic Devices. *J. Appl. Phys.* **2000**, *87*, 2542−2547.

(18) Brea, R. J.; Pérez-Alvite, M. J.; Panciera, M.; Mosquera, M.; Castedo, L.; Granja, J. R. Highly Efficient and Directional Homo-and Heterodimeric Energy Transfer Materials Based on Fluorescently Derivatized α,γ-Cyclic Octapeptides. *Chem. - Asian J.* **2011**, *6*, 110−121.

(19) Sun, Q.; Cai, L. L.; Ma, H. H.; Yuan, C. X.; Xu, W. Dehalogenative Homocoupling of Terminal Alkynyl Bromides on Au(111): Incorporation of Acetylenic Scaffolding into Surface Nanostructures. *ACS Nano* **2016**, *10*, 7023−7030.

(20) Stepanow, S.; Lingenfelder, M.; Dmitriev, A.; Spillmann, H.; Delvigne, E.; Lin, N.; Deng, X. B.; Cai, C. Z.; Barth, J. V.; Kern, K. Steering Molecular Organization and Host-Guest Interactions Using Two-Dimensional Nanoporous Coordination Systems. *Nat. Mater.* **2004**, *3*, 229−233.

(21) Lingenfelder, M. A.; Spillmann, H.; Dmitriev, A.; Stepanow, S.; Lin, N.; Barth, J. V.; Kern, K. Towards Surface-Supported Supramolecular Architectures: Tailored Coordination Assembly of 1,4-Benzenedicarboxylate and Fe on Cu(100). *Chem. - Eur. J.* **2004**, *10*, 1913−1919.

(22) Liu, J.; Lin, T.; Shi, Z. L.; Xia, F.; Dong, L.; Liu, P. N.; Lin, N. Structural Transformation of Two-Dimensional Metal-Organic Coordination Networks Driven by Intrinsic in-Plane Compression. *J. Am. Chem. Soc.* **2011**, *133*, 18760−18766.

(23) Stepanow, S.; Lin, N.; Payer, D.; Schlickum, U.; Klappenberger, F.; Zoppellaro, G.; Ruben, M.; Brune, H.; Barth, J. V.; Kern, K. Surface-Assisted Assembly of 2D Metal-Organic Networks That Exhibit Unusual Threefold Coordination Symmetry. *Angew. Chem., Int. Ed.* **2007**, *46*, 710−713.

(24) Hanke, F.; Haq, S.; Raval, R.; Persson, M. Heat-to-Connect: Surface Commensurability Directs Organometallic One-Dimensional Self-Assembly. *ACS Nano* **2011**, *5*, 9093−9103.

(25) Haq, S.; Hanke, F.; Dyer, M. S.; Persson, M.; Iavicoli, P.; Amabilino, D. B.; Raval, R. Clean Coupling of Unfunctionalized Porphyrins at Surfaces to Give Highly Oriented Organometallic Oligomers. *J. Am. Chem. Soc.* **2011**, *133*, 12031−12039.

(26) Liu, J.; Chen, Q.; Xiao, L.; Shang, J.; Zhou, X.; Zhang, Y.; Wang, Y.; Shao, X.; Li, J.; Chen, W.; et al. Lattice-Directed Formation of Covalent and Organometallic Molecular Wires by Terminal Alkynes on Ag Surfaces. *ACS Nano* **2015**, *9*, 6305−6314.

(27) Graziosi, P.; Riminucci, A.; Prezioso, M.; Newby, C.; Brunel, D.; Bergenti, I.; Pullini, D.; Busquets-Mataix, D.; Ghidini, M.; Dediu, V. A. Pentacene Thin Films on Ferromagnetic Oxide: Growth Mechanism and Spintronic Devices. *Appl. Phys. Lett.* **2014**, *105*, 022401.

(28) Roelofs, W. S. C.; Charrier, D. S. H.; Dzwilewski, A.; Janssen, R. A. J.; de Leeuw, D. M.; Kemerink, M. Scanning Tunnelling Microscopy on Organic Field-Effect Transistors Based on Intrinsic Pentacene. *Appl. Phys. Lett.* **2014**, *104*, 263301.

(29) Hutchins, D. O.; Weidner, T.; Baio, J.; Polishak, B.; Acton, O.; Cernetic, N.; Ma, H.; Jen, A. K. Y. Effects of Self-Assembled Monolayer Structural Order, Surface Homogeneity and Surface Energy on Pentacene Morphology and Thin Film Transistor Device Performance. *J. Mater. Chem. C* **2013**, *1*, 101−113.

(30) Congreve, D. N.; Lee, J. Y.; Thompson, N. J.; Hontz, E.; Yost, S. R.; Reusswig, P. D.; Bahlke, M. E.; Reineke, S.; Van Voorhis, T.; Baldo, M. A. External Quantum Efficiency above 100% in a Singlet-Exciton-Fission-Based Organic Photovoltaic Cell. *Science* **2013**, *340*, 334−337.

(31) Liu, C.; Xu, Y.; Noh, Y. Y. Contact Engineering in Organic Field-Effect Transistors. *Mater. Today* **2015**, *18*, 79−96.

(32) Huang, Z. Y.; Simpson, D. E.; Mahboub, M.; Li, X.; Tang, M. L. Ligand Enhanced Upconversion of Near-Infrared Photons with Nanocrystal Light Absorbers. *Chem. Sci.* **2016**, *7*, 4101−4104.

(33) Fenwick, O.; Van Dyck, C.; Murugavel, K.; Cornil, D.; Reinders, F.; Haar, S.; Mayor, M.; Cornil, J.; Samorì, P. Modulating the Charge Injection in Organic Field-Effect Transistors: Fluorinated Oligophenyl Self-Assembled Monolayers for High Work Function Electrodes. *J. Mater. Chem. C* **2015**, *3*, 3007−3015.

DOI: 10.1021/acs.jpcc.7b03957
J. Phys. Chem. C 2017, 121, 21650−21657

(34) Cun, H.; Wang, Y.; Du, S.; Zhang, L.; Zhang, L.; Yang, B.; He, X.; Wang, Y.; Zhu, X.; Yuan, Q.; et al. Tuning Structural and Mechanical Properties of Two-Dimensional Molecular Crystals: The Roles of Carbon Side Chains. *Nano Lett.* **2012**, *12*, 1229−34.
(35) Repp, J.; Meyer, G.; Paavilainen, S.; Olsson, F. E.; Persson, M. Imaging Bond Formation between a Gold Atom and Pentacene on an Insulating Surface. *Science* **2006**, *312*, 1196−1199.
(36) Wu, R.; Yan, L.; Zhang, Y.; Ren, J.; Bao, D.; Zhang, H.; Wang, Y.; Du, S.; Huan, Q.; Gao, H.-J. Self-Assembled Patterns and Young's Modulus of Single-Layer Naphthalocyanine Molecules on Ag(111). *J. Phys. Chem. C* **2015**, *119*, 8208−8212.
(37) Vanderbilt, D. Soft Self-Consistent Pseudopotentials in a Generalized Eigenvalue Formalism. *Phys. Rev. B: Condens. Matter Mater. Phys.* **1990**, *41*, 7892−7895.
(38) Kresse, G.; Joubert, D. From Ultrasoft Pseudopotentials to the Projector Augmented-Wave Method. *Phys. Rev. B: Condens. Matter Mater. Phys.* **1999**, *59*, 1758−1775.
(39) Perdew, J. P.; Burke, K.; Ernzerhof, M. Generalized Gradient Approximation Made Simple. *Phys. Rev. Lett.* **1996**, *77*, 3865−3868.
(40) Perdew, J. P.; Chevary, J. A.; Vosko, S. H.; Jackson, K. A.; Pederson, M. R.; Singh, D. J.; Fiolhais, C. Atoms, Molecules, Solids, and Surfaces: Applications of the Generalized Gradient Approximation for Exchange and Correlation. *Phys. Rev. B: Condens. Matter Mater. Phys.* **1992**, *46*, 6671−6687.
(41) Wu, X.; Vargas, M. C.; Nayak, S.; Lotrich, V.; Scoles, G. Towards Extending the Applicability of Density Functional Theory to Weakly Bound Systems. *J. Chem. Phys.* **2001**, *115*, 8748−8757.
(42) Ocko, B. M.; Helgesen, G.; Schardt, B.; Wang, J.; Hamelin, A. Charge Induced (1 × 3) Reconstruction of the Au(110) Surface: An X-ray Scattering Study. *Phys. Rev. Lett.* **1992**, *69*, 3350−3353.
(43) Floreano, L.; Cossaro, A.; Cvetko, D.; Bavdek, G.; Morgante, A. Phase Diagram of Pentacene Growth on Au(110). *J. Phys. Chem. B* **2006**, *110*, 4908−4913.
(44) Guaino, P.; Carty, D.; Hughes, G.; McDonald, O.; Cafolla, A. A. Long-Range Order in a Multilayer Organic Film Templated by a Molecular-Induced Surface Reconstruction: Pentacene on Au(110). *Appl. Phys. Lett.* **2004**, *85*, 2777−2779.
(45) Bavdek, G.; Cossaro, A.; Cvetko, D.; Africh, C.; Blasetti, C.; Esch, F.; Morgante, A.; Floreano, L. Pentacene Nanorails on Au(110). *Langmuir* **2008**, *24*, 767−772.
(46) Evangelista, F.; Ruocco, A.; Pasca, D.; Baldacchini, C.; Betti, M. G.; Corradini, V.; Mariani, C. Au(110) Induced Reconstruction by π Conjugated Molecules Adsorption Investigated by Photoemission Spectroscopy and Low Energy Electron Diffraction. *Surf. Sci.* **2004**, *566-568*, 79−83.
(47) Corradini, V.; Menozzi, C.; Cavallini, M.; Biscarini, F.; Betti, M. G.; Mariani, C. Growth Morphology and Electronic Structure of 2D Ordered Pentacene on the Au(110)-(1 × 2) Surface. *Surf. Sci.* **2003**, *532-535*, 249−254.
(48) Baldacchini, C.; Mariani, C.; Betti, M. G. Adsorption of Pentacene on Filled D-Band Metal Surfaces: Long-Range Ordering and Adsorption Energy. *J. Chem. Phys.* **2006**, *124*, 154702.
(49) Cui, P.; Zhang, Q.; Zhu, H. B.; Li, X. X.; Wang, W. Y.; Li, Q. X.; Zeng, C. G.; Zhang, Z. Y. Carbon Tetragons as Definitive Spin Switches in Narrow Zigzag Graphene Nanoribbons. *Phys. Rev. Lett.* **2016**, *116*, 026802.
(50) Korventausta, A.; Paavilainen, S.; Niemi, E.; Nieminen, J. A. Stm Simulation of Molecules on Ultrathin Insulating Overlayers Using Tight-Binding: Au−Pentacene on NaCl Bilayer on Cu. *Surf. Sci.* **2009**, *603*, 437−444.

DOI: 10.1021/acs.jpcc.7b03957
J. Phys. Chem. C 2017, 121, 21650−21657